Analysis of grain-boundary structure in Al–Cu interconnects

David P. Field
TexSEM Laboratories, Inc., 226W 2230N, Provo, Utah 84604

John E. Sanchez, Jr.
Department of Materials Science and Engineering, University of Michigan, Ann Arbor, Michigan 48109-2136

Paul R. Besser
Advanced Micro Devices, Sunnyvale, California 94088-3453

David J. Dingley
TexSEM Laboratories, Inc., 226W 2230N, Provo, Utah 84604

(Received 31 March 1997; accepted for publication 9 June 1997)

The role of crystallographic texture in electromigration resistance of interconnect lines is well documented. The presence of a strong (111) fiber texture results in a more reliable interconnect structure. It is also generally accepted that grain-boundary diffusion is the primary mechanism by which electromigration failures occur. It has been difficult to this point, however, to obtain statistically reliable information of grain-boundary structure in these materials as transmission electron microscopy investigations are limited by tedious specimen preparation and small, nonrepresentative, imaging regions. The present work focuses upon characterization of texture and grain-boundary structure of interconnect lines using orientation imaging microscopy, and particularly, upon the linewidth dependence of these measures. Conventionally processed Al–1%Cu lines were investigated to determine the affects of a postpatterning anneal on boundary structure as a function of linewidth. It was observed that texture tended to strengthen slightly with decreasing linewidth subsequent to the anneal procedure. Grain morphology changed substantially as the narrow lines became near bamboo in character and the crystallographic character of the boundary plane changed as a function of linewidth. These results are contrasted with those obtained from Al–1%Cu lines, which were fabricated using the damascene process. The damascene lines show a marked weakening in texture as the linewidth decreases, accompanied by a more random misorientation distribution. A description of the competing energetics, which result in the observed microstructures, is included. © *1997 American Institute of Physics.* [S0021-8979(97)08617-9]

I. INTRODUCTION

The phenomenon of electromigration in interconnect lines of integrated circuit structures has been investigated extensively during the past three decades. As the feature size of these interconnects continues to shrink and current density increases, optimization of the microstructure for electromigration resistance becomes increasingly important. Among other factors, crystallographic texture has been shown to play a key role in extending the lifetime of interconnect structures operating under conditions where electromigration dominates, as well as resisting stress voiding and hillock formation. It is known that the presence of a strong (111) fiber texture normal to the plane of the metallization layer is desirable.[1–4] This result has been obtained for Al–Cu, Al–Si, Al–Cu–Si, and Cu systems. Electromigration occurs as a result of diffusion processes induced by the ''electron wind'' forces, which have mass flux, primarily along grain boundaries in nonbamboo-type interconnects. The strong dependence on crystallographic texture can be rationalized in terms of the constraint such textures place on grain-boundary structure. Some investigators have argued that (111)-oriented grains might be expected to have a more uniform distribution of grain-boundary diffusivities, owing to the narrower range of structural possibilities.[2,4,5] It follows that controlling the crystallographic character of the boundary structure, or microtexture, in a material may be a more robust tool for optimizing performance than that of merely controlling the average film texture. Recent efforts in Russia have shown a significant difference in electromigration activation energies for differing deposition parameters using the partially ionized beam technique [cf. Ref. 6]. The observed differences were explained on the basis of grain-boundary structure arguments, though no measurements of the microtexture were made to substantiate the claim.

Until recently, a reliable technique for measuring these microtextural parameters of the structure was unavailable and little effort was made toward measuring the statistical distribution of grain-boundary character. Manual transmission electron microscopy (TEM) based methods reveal a wealth of information but are restricted in their usefulness by cumbersome specimen preparation procedures and limited analysis regions from each specimen. The development of automated analysis procedures, particularly that of orientation imaging microscopy in the scanning electron microscope (SEM),[7–9] has begun to overcome these difficulties to the extent that realistic microtextural measures can now be obtained over relatively large areas. The present work focuses upon a comparison of the texture and grain-boundary character distribution of a conventionally processed interconnect test structure with similar information from a test struc-

ture created using a damascene fabrication process.

II. EXPERIMENTAL DETAILS

Two types of Al–1%Cu specimens were prepared for this investigation. The first consisted of a metallization layer, which was patterned into a test structure of interconnect lines having various widths using conventional fabrication procedures (metal deposition-pattern-etch). The lines ranged from 8.0 to 0.75 μm in width. A postpatterning anneal was then applied to determine its effects on the texture and grain-boundary structure of lines having various widths. The resulting structures showed a near-bamboo character for those lines having widths less than 2.0 μm. The second set of specimens consisted of lines fabricated using the damascene process (oxide–deposition-pattern-etch–metal fill-chemical–mechanical polish). This process consisted of etching 1.0 μm deep trenches with essentially vertical sidewalls. A wetting layer that included a thin Ti layer in contact with the Al was used in the process. The deposition process was observed to completely fill the trenches with the Al–Cu material. The chemical–mechanical polishing procedure revealed the resulting lines, which had widths ranging from 8.0 to 0.5 μm.

These structures were investigated using orientation imaging microscopy (OIM). This technique has been shown to be reliable in investigating thin-film structures with grain sizes on the order of 0.25 μm or greater.[10–13] OIM is a process based on electron backscatter diffraction (EBSD) in the SEM. Using OIM, computer generated maps of the crystallographic morphology of a material are constructed and a number of microstructural measures can be extracted directly from the data. Since the crystallographic information is inherently collected during the imaging process, a substantial amount of spatially specific information is rapidly obtained. Details of the technique are found elsewhere[7–9] and will not be included in the present discussion. OIM requires no special specimen preparation techniques for thin-film metallizations and patterned structures. The passivation layer typically present on such structures must be removed, however, for EBSD investigations. No passivation layer was deposited during the fabrication processes for any of the specimens analyzed in the present investigation.

Analyses were performed on the crystallographic texture of the interconnect lines. Orientation distribution functions (ODFs) were calculated using a binning procedure for discrete orientation measurements similar to that described by Matthies and Vinel.[14] Pole figures and one-dimensional pole plots were recalculated from the ODFs obtained for comparative evaluation. Grain-boundary structure was analyzed using the assumption that all boundaries were aligned normal to the plane of the deposited films, and so the two-dimensional views seen by OIM are assumed representative of the three-dimensional structure. Although such an assumption is not universally accurate, energetic arguments can be used to justify such an assumption. Minimization of interface energy generally requires the smallest possible boundary area, which is the reason bamboo-type structures commonly occur when geometric constraints are removed. The through thickness inclination of the boundary is energetically unfavorable and can occur in an equilibrium structure only under conditions of additional constraints. The crystallographic plane aligned with the boundary plane on either side of the boundary was measured using this assumption. Misorientation distributions were measured directly from the data using both the spatially correlated information and the more conventional uncorrelated assumption.[15,16]

III. RESULTS

A. Conventionally fabricated specimens

The goal of the investigation for these specimens was to determine the effect of a postpatterning anneal on the evolution of texture and grain-boundary structure. The ideal experiment would include an analysis of the crystallite morphology prior to patterning and annealing, and a subsequent analysis after the process. Since this type of experiment was not realistic with the available resources, a patterned and annealed material was analyzed for differences in texture and boundary structure as a function of feature size. This is based on the assumption that structural evolution occurs during the anneal, and that differing geometric constraints on the process (linewidths) would yield differing results. Results from the texture study have been previously reported,[17] but are briefly summarized here to aid in the understanding of the grain-boundary structure.

OIM maps were obtained from narrow lines, wide lines, and pad-type regions of the specimens. All lines and pads investigated were from the same region of each specimen. Figure 1 shows a typical OIM image of a region of the structure with shading according to crystallite lattice orientation. Wide and narrow lines are shown in the image. The black shaded regions are those between the interconnect lines. Different gray scales on the metal lines indicate the degree of misorientation from an ideal (111) fiber orientation. The darker shaded regions indicate crystallites within 5° misorientation of the (111) fiber, while the lighter shaded regions are those between 5° and 10° misoriented from the ideal position. Unshaded regions are misoriented more than 10° from (111). Grain boundaries are defined in this image as misorientations between neighboring measurements of 5° or greater and thin black lines are used to indicate the boundary positions.

The texture of this material is indicated by the (111) pole figures shown in Fig. 2. These plots are stereographic projections of the (111) crystallographic plane normal orientation distributions. The center of the plots is the position normal to the specimen surface. These figures were recalculated from the complete ODF determined from the individual measurements. Fig. 2(a) contains the distribution for the pad regions, Fig. 2(b) for the wide line regions, and Fig. 2(c) for the narrow lines. All regions contain sharp (111) textures, but the distribution for the narrow lines is slightly stronger than that for the wide lines, which is stronger than that for the pad regions as indicated by the maximum value shown in each of the pole figures. This value is in units of times random. Similar information can be seen in the form of (111) pole plots, which integrate about the azimuthal angle of the pole figures, assuming a perfect fiber texture. Such a plot of all three distributions is contained in Fig. 3. This type of

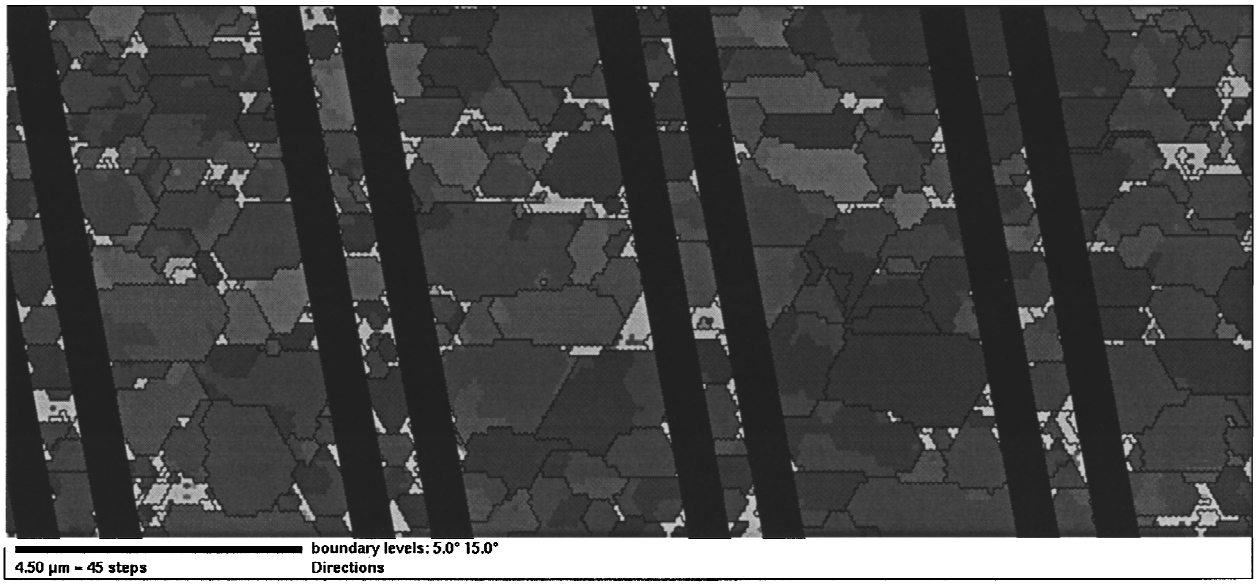

FIG. 1. Orientation image of a patterned test structure showing orientation dependence of narrow and wide lines.

texture representation appears similar to conventional rocking curves obtained by x-ray diffraction techniques.

The morphology of the grain-boundary structure was used in determining the difference between wide and narrow lines. The narrow lines are defined as those that are near bamboo in structure (less than about 2 μm) while the wide lines, typically, contain more than one grain across the linewidth. The grain-boundary structure distribution can be shown using a variety of graphical representations. The simplest of these is the misorientation angle histogram, or Mackenzie plot.[18] Figure 4 shows the misorientation angle dependence on linewidth for this material. The trend seen in Fig. 4 is for the narrow lines to have a shift towards low angle boundaries, while the wider lines are shifted to a distribution weighted heavier in high angle misorientations. This can be significant as much evidence exists that low angle boundaries are low-energy and low diffusivity positions[19–23] and are, therefore, more stable under integrated circuit (IC) operating conditions.

A more complete representation of the misorientation distribution could be made to show the axis of rotation as well as the rotation angle. In the case of the textures investigated here, however, the presence of the strong (111) fiber texture leads to the result that virtually all boundaries are misoriented about the [111] axis. This result is consistent for all three pattern geometries considered here. The crystallographic plane, which coincides with the grain-boundary plane for each boundary is also of primary importance in characterizing the boundary structure. Since the strong fiber texture exists, and the assumption of having the boundary plane normal to the metal layer has been made, the possible positions of the boundary plane are restricted. Figure 5 shows the distribution of the crystallographic orientations coincident with the plane normal orientations. There are two points in the unit triangle for each boundary as the crystallite on either side is considered independently. Figure 5(a) shows the distribution for wide lines while that for the narrow lines is shown in Fig. 5(b). The distribution for the wide lines is somewhat randomly distributed throughout the possible region [an arc extending from the [101] position to the [112] position where the condition $(111)\cdot(hkl)=0$ must be satisfied]. The distribution for the narrow lines is weighted more heavily near the (110)-type planes. Quantitative analysis reveals that approximately twice as many boundaries lie within 15° of the (110) plane than the (112) plane for the narrow lines. The morphology of these structures is primarily bamboo in character, so the predominance of a given class of planes suggest some in-plane preferred orientation of the texture distribution. The in-plane preference is observed to a certain extent in the pole figure shown in Fig. 2(c) for the narrow lines. This suggests that the texture evolution and grain-boundary plane evolution to a lower energy state during the postpatterning anneal involves the preferred growth of low-energy crystallites so the near (110) planes align with the bamboo structure.

Coincident site lattice (CSL) theory[24] was used in determining the grain-boundary character distribution. Brandon's criterion[25] was used in the investigation. The large majority of CSL-type misorientations present in the structure are defined by rotations about the ⟨111⟩ axis. Ideal (111) fiber textured specimens are composed entirely of (111) tilt boundaries, so the grain-boundary plane does not align with the high-density plane of coincident lattice sites for those defined by rotations about the ⟨111⟩ axis. Additional planes exist, which contain periodic arrays of coincident sites, such as the (211) for the $\Sigma 3$ boundary, but these are higher energy boundaries. When the orientation of the boundary plane is considered as part of the specialness criteria (cf. Ref. 26), there were no CSL boundaries in the structure with the exception of the low angle ($\Sigma 1$) boundaries.

B. Damascene process fabricated specimens

The processing and crystallographic texture of the damascene specimens is discussed elsewhere[27,28] and will not be

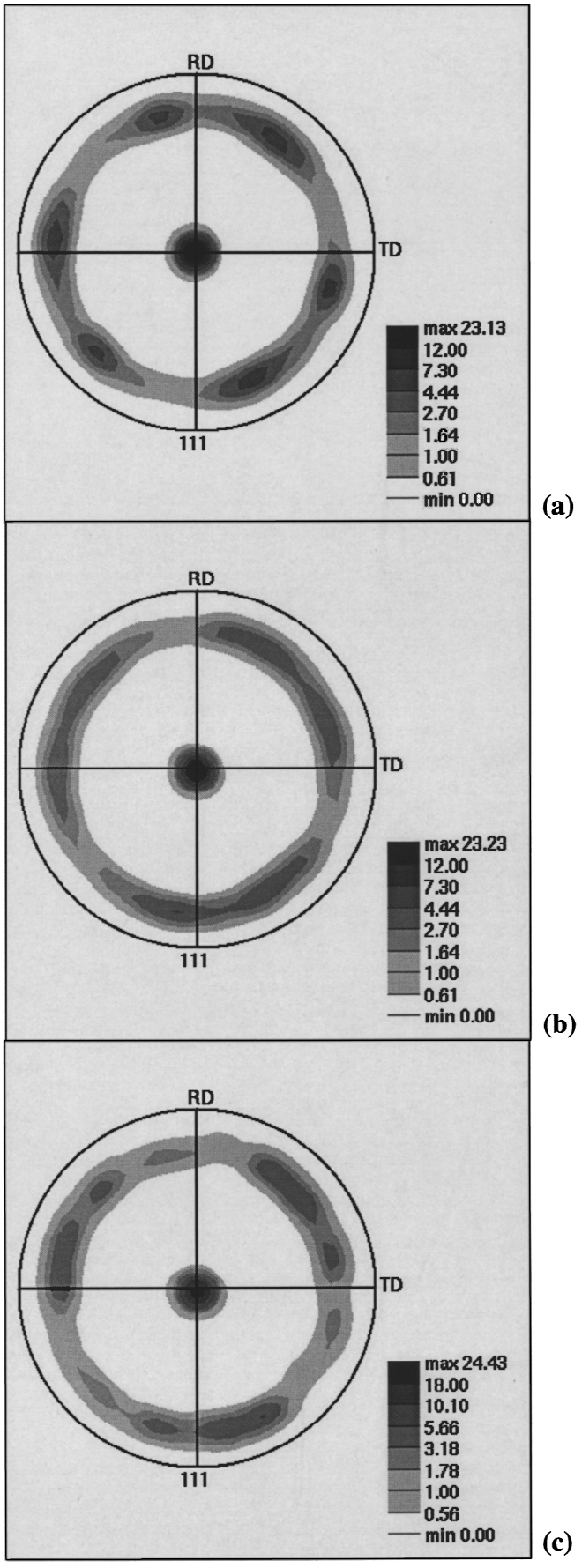

FIG. 2. (111) pole figures for (a) unpatterned region, (b) wide lines, and (c) narrow lines.

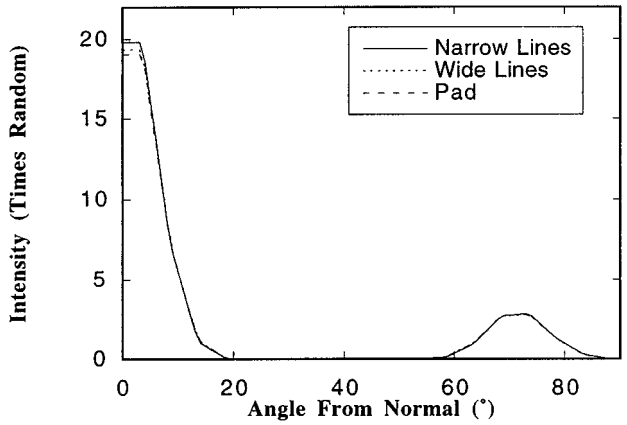

FIG. 3. Pole plot histogram showing relative (111) fiber texture strengths of the various features.

described in detail in the present work. Figures 6 and 7 show OIM images created from the data for the 8 μm wide lines and the 0.5 μm wide lines, respectively. The middle line seen in Fig. 6 shows a somewhat distorted view of one of the 8 μm lines. This distortion is caused by electronic and/or mechanical drift in the SEM during an overnight imaging period. The width of the 0.5 μm lines appears to be closer to 1.0 μm than 0.5 μm in the image seen in Fig. 7. This is because the lines were inclined 70° from horizontal for OIM analysis and the resolution of the tungsten source SEM for EBSD analysis is on the order of 0.25 μm, giving a spread in the data on either side of the interconnect line. The crystallographic texture of the damascene process fabricated specimens is indicated by the (111) pole plot shown in Fig. 8. These curves were recalculated from the complete ODF determinations. It is apparent that the trend is for much weaker textures present in the narrow lines as compared to the relatively strong textures seen in the wider lines. The 0.5 μm lines also contain a significant (100) orientation component, which is not present in the wider lines.

The grain-boundary structure as characterized by Mackenzie plots is quite different from that which might be expected from analysis of the orientation distribution. Figure 9 shows a comparison between the texture derived misorienta-

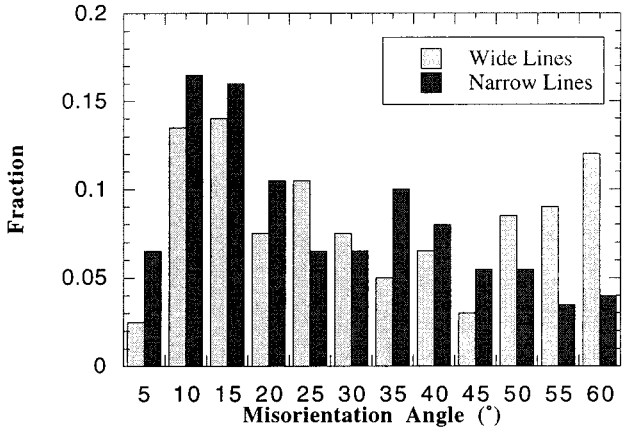

FIG. 4. Mackenzie plot (misorientation angle histogram) of wide and narrow interconnect lines.

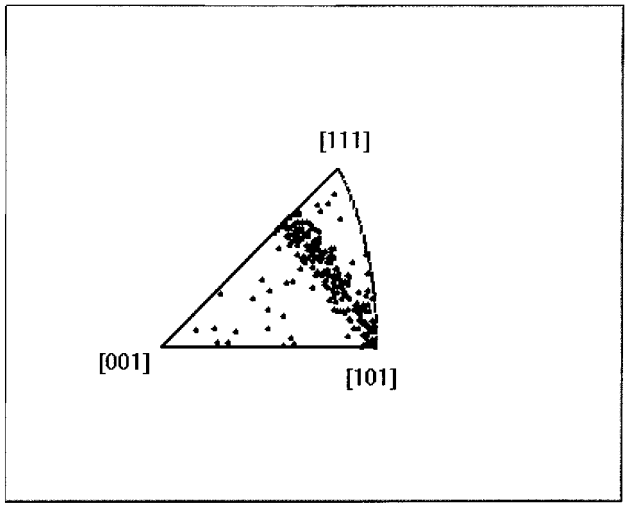

(a)

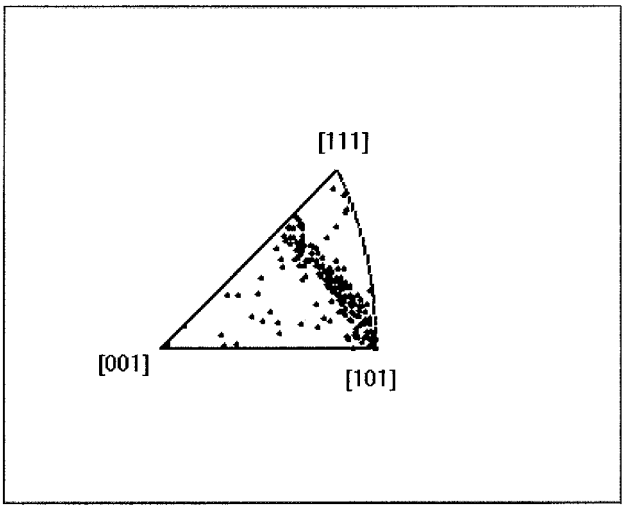

(b)

FIG. 5. Unit triangle showing the lattice planes which align with the grain boundary for (a) the wide lines and (b) the narrow lines.

tion angle distribution and the measured distribution from OIM data for the 8 μm wide specimens. The texture derived distribution assumes no spatial correlation of orientations. In other words, the texture components are assumed to occur randomly throughout the material. The distribution obtained from OIM data is that found from actual measurements of relative orientations from grain to grain in the specimen. In all linewidths, the results are similar in that a much higher fraction of low angle boundaries exists as seen by direct measurements than would be expected for randomly distributed texture components. This holds true even at narrow linewidths where the texture of the lines is weak and the misorientation angle distribution might be expected to be similar to the Mackenzie plot for completely random textures.[18]

The complete misorientation distribution functions show a significant fraction of neighboring crystallite orientations rotated about $\langle 111\rangle$-type axes with respect to one another. The $\langle 111\rangle$ boundaries are strongest for the stronger textures and weaker as linewidth, and texture strength, decreases.

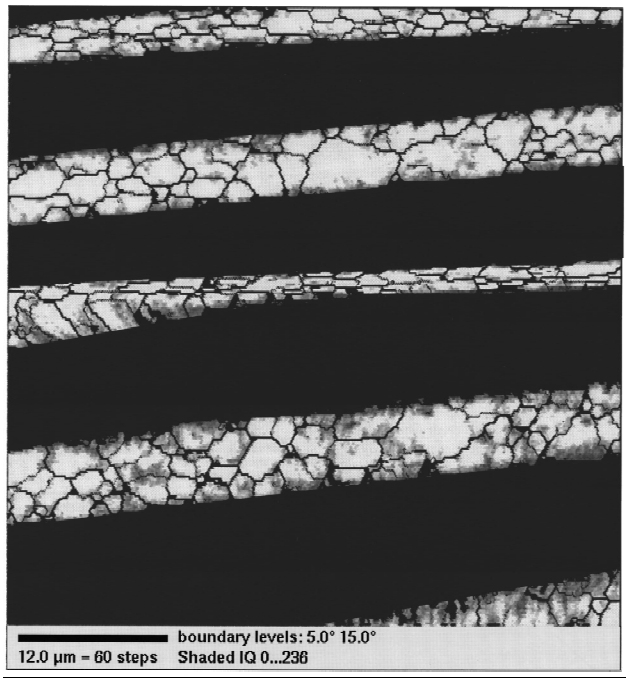

FIG. 6. Orientation image showing structure of 8.0 μm wide damascene process fabricated lines.

This is most readily seen in the asymmetric domain for misorientations plotted in the Rodrigues space representation (cf. Refs. 29 and 30). Rodrigues vectors lie in a three-dimensional space defined by $\mathbf{r}=\mathbf{n}\tan\omega/2$ where $\mathbf{n}$ is a unit vector describing the rotation axis between neighboring crystallites and ω is the angle of rotation. Figure 10 shows a comparison of the misorientation distribution functions (MDFs) between the 8 μm wide lines and the 0.5 μm wide lines (the two extreme cases for this investigation). The asymmetric domain for misorientations between crystallites having cubic symmetry is shown. The lower left-hand corner of the box labeled $r_3=0.015$ is the origin of the space and the lower left-hand corner of the increasingly smaller triangle in each r_3 section is the position of the $\langle 111\rangle$ rotation axis. The distribution for the 8 μm wide lines is concentrated around the $\langle 111\rangle$ axis with only a small peak in the distribution at a position approximately 60° rotated about a $\langle 110\rangle$ axis (upper right-hand corner of the $r_3=0.015$ section). The 0.5 μm line MDF shows a substantial amount of off-$\langle 111\rangle$-axis misorientation relationships. These correspond to boundaries between (111)- and (100)-oriented grains. The distribution also contains a significant fraction of $\langle 111\rangle$ rotations between neighboring crystallites. The 60° $\langle 110\rangle$ misorientation seen in the 8 μm line MDF appears with more strength in the narrow lines. This relationship will be discussed in the following section.

The position of the grain-boundary plane with respect to the crystallite lattices on either side of the boundary is another important consideration in defining the character of grain boundaries in the structure. As mentioned above, the distribution of lattice planes, which lie coincident with a grain-boundary plane for an ideal (111) fiber texture is known to be an are tracing from the (110) plane to the (112) plane. In the case of the damascene process fabricated lines,

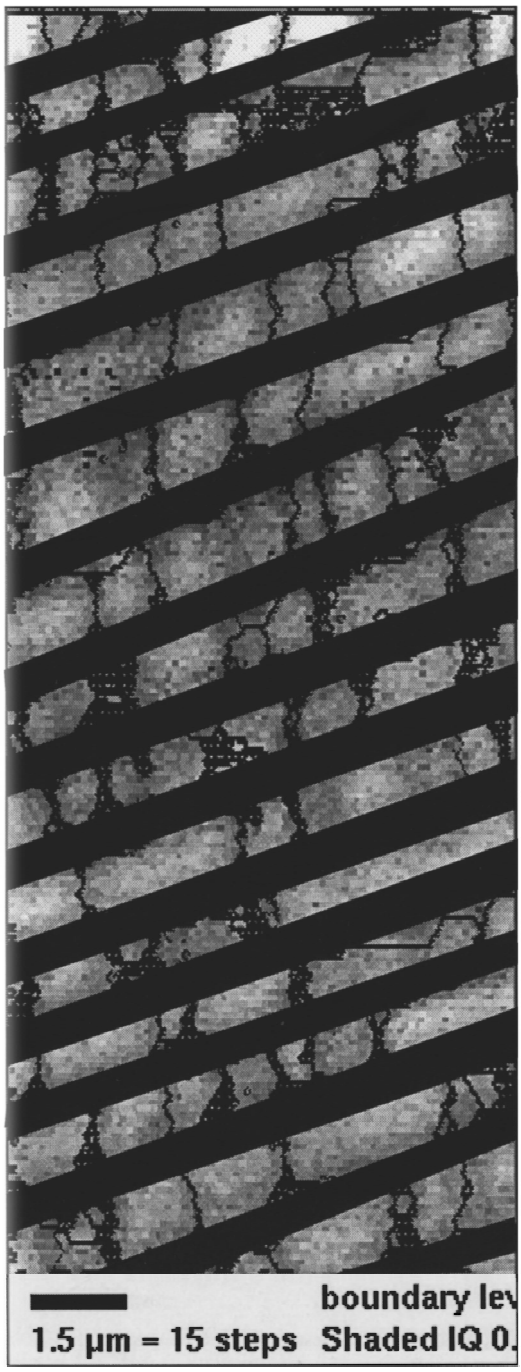

FIG. 7. Orientation image showing structure of 0.5 μm wide damascene process fabricated lines.

the textures are strongest for wide lines and weaker for the narrow lines. Again, we assume that the boundary planes lie normal to the specimen surface. The corresponding distribution of crystallite lattice planes is consistent with the ideal case. The narrow lines have a weaker distribution, but retain the character of the stronger textured 8 μm lines in that most of the distributions tend to be shifted towards the (110) position as opposed to the (112). Figure 11 contains the distribution for the 8 μm lines as compared with that for the 1 μm lines, which is the most random distribution observed of lattice planes aligned with the grain-boundary plane.

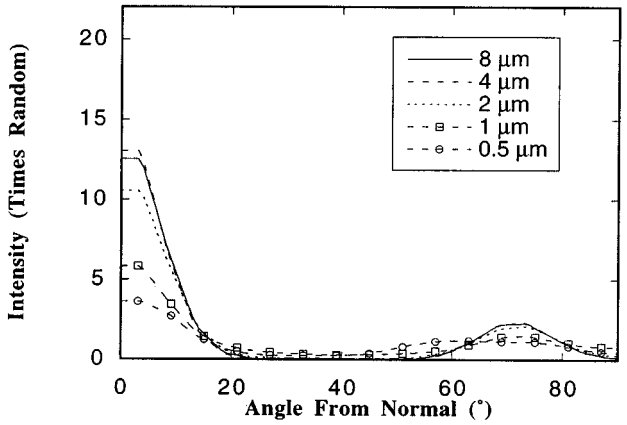

FIG. 8. (111) pole plot showing fiber texture strength of the damascene lines as a function of width.

IV. DISCUSSION

The ability to obtain large amounts of spatially specific crystallite lattice orientation information by OIM enables complete characterization of the crystallographic morphology of materials. Bulk texture distributions and specific microtextural relationships are inherently obtained in the data collection procedure. From the studies described in the present work, a comparison between the textures and the grain-boundary character of conventionally processed interconnect lines and damascene process fabricated lines is possible.

All specimens examined in this work exhibited a (111) fiber texture of varying strength. For the conventionally processed lines, the postannealing strength of texture increased as the linewidth decreased. This was not a large effect, but was consistent in all analyses made. This can be explained in terms of the geometric constraints of postpatterning structure evolution. As the linewidth decreases, the constraints on boundary motion are reduced and the structure can achieve a lower energy state by allowing the lower energy (111) grains to preferentially grow at the expense of grains that are less favorably oriented. Surface energy (cf. Ref. 31) of the unpassivated line sidewalls becomes more significant as linewidth

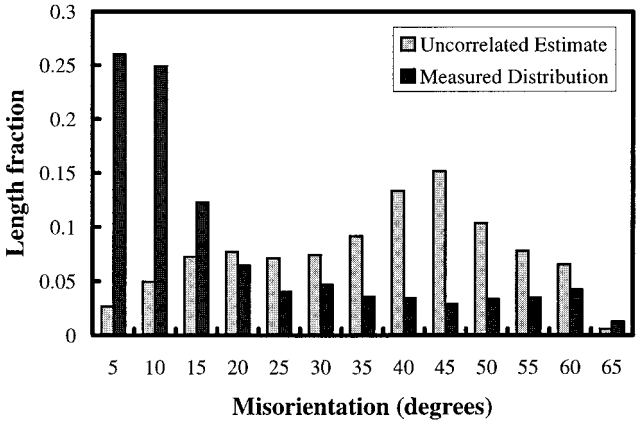

FIG. 9. Mackenzie plots of 8.0 μm wide lines showing the contrasting character of the (a) uncorrelated MDF calculation, with (b) that obtained from OIM data.

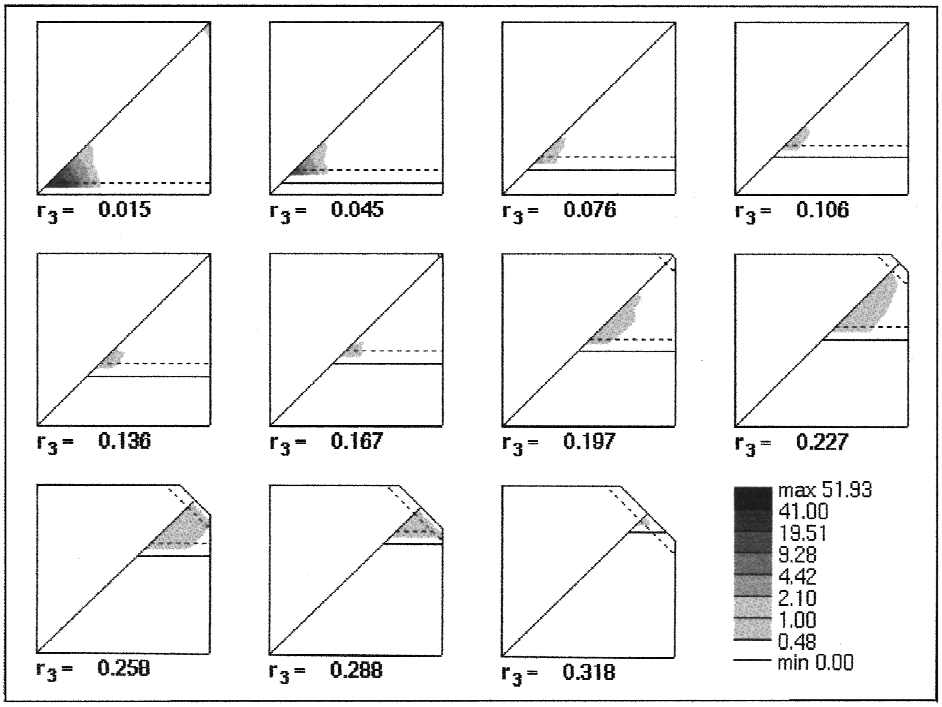

(a)

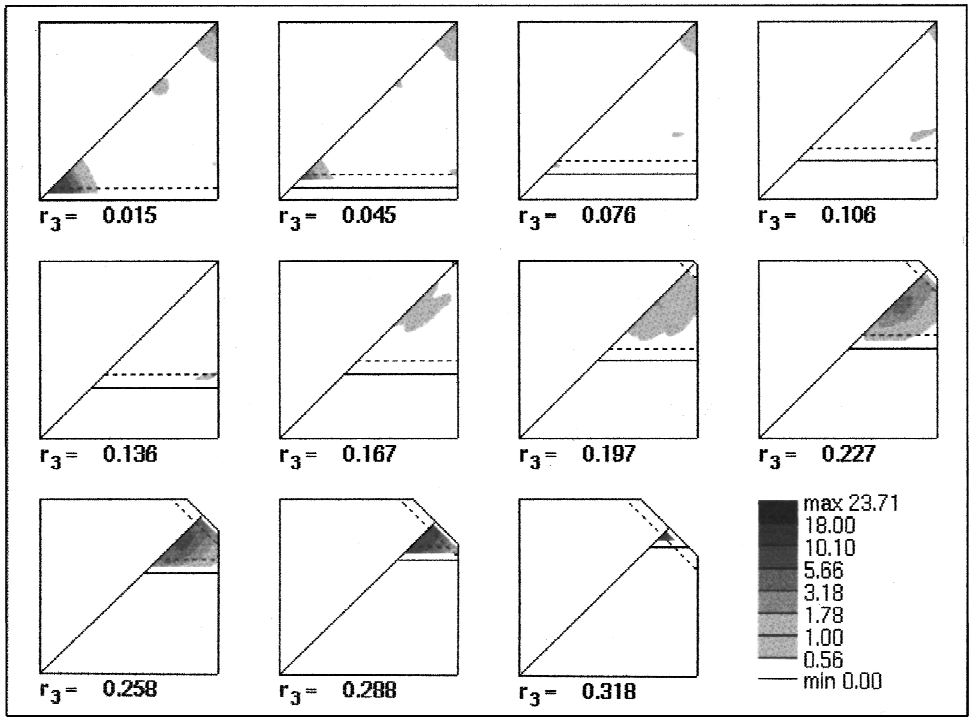

(b)

FIG. 10. Rodrigues space representations of the misorientation distribution for (a) the 8.0 μm wide lines and (b) the 0.5 μm wide lines.

decreases. In addition, grain-boundary energy minimization will play a role in assisting or hindering the process. These considerations are discussed below. Elastic strain energy minimization results in a (100) texture for the Al–Cu system at temperatures below a critical value. At the higher temperatures involved in the postpatterning anneal procedure, however, the surface and interface energy minimization dominate the process, resulting in the observed (111) texture (cf. Ref. 32). Regardless of this observation, residual stresses cannot be discounted as contributing to the observed phenomena.

The grain-boundary structure dependence on linewidth for both types of specimens was apparent from the results. Mackenzie plots showed a definite propensity for the conventionally processed narrow lines to have a large fraction of low angle boundaries as compared with the wider lines. A similar result was observed by Knorr and Rodbell[4] for con-

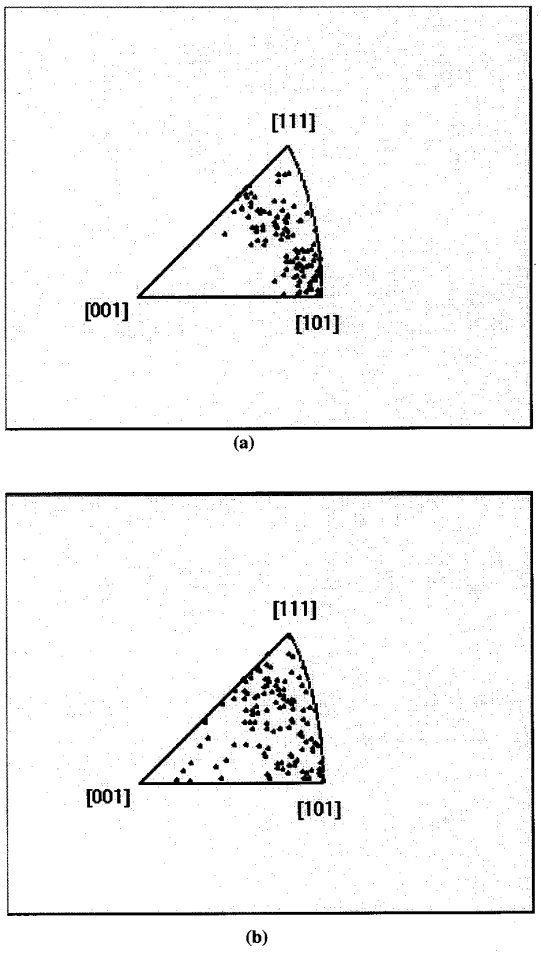

FIG. 11. Unit triangles showing the distribution of lattice planes aligned with the grain boundary for (a) the 8.0 μm lines and (b) the 1.0 μm lines.

ventionally processed lines where a larger than expected fraction of low angle boundaries was measured by EBSD and TEM analyses. Energetic arguments can be used to explain this result in a similar manner to that for the bulk texture. Low angle boundaries have long been known to be in a more stable, low-energy configuration.[22,33] As the structure evolves and seeks the lowest energy configuration, these low angle boundaries are more favorable in the absence of competing effects. Constraints on the system of interface area and neighboring lattice orientation are decreased with decreasing linewidths.

In the absence of additional constraints, grain-boundary area minimization requires the development of a bamboo structure in IC interconnect lines. Constraints to the development of bamboo structure are imposed by metal/oxide interfaces, neighboring grains, grain-boundary energy requirements, and grain size considerations. As the lines become more narrow, the constraints are reduced and the bamboo structure can be more readily achieved. Grain-boundary energy, γ_{gb}, is a function of the geometric parameters of the crystallite lattice orientations and the boundary plane orientation. (Chemistry and local crystallite structure also play important roles, but can be assumed constant for this problem.) As the position of the boundary migrates, driven by boundary area minimization, towards the minimum area position, the plane necessarily sweeps through various boundary structures, which correspond to varying boundary energies.

Grain-boundary migration is a result of grain growth mechanisms where the boundary energy, E_{gb}, and mobility, M, control the process. The velocity of the grain-boundary motion is given by

$$\nu = M E_{gb} \kappa,$$

where κ is the boundary curvature. As boundary energy is minimized, the velocity decreases and the boundary reaches an equilibrium position. The total energy of the grain boundary, E_{gb}, can be expressed by integrating the specific boundary energy, γ_{gb}, over the area of the boundary (taking into account the variability in boundary normal orientation) as follows:

$$E_{gb} = \int_A \gamma_{gb}(g, \mathbf{n}, g') dA(\mathbf{n}).$$

The specific grain-boundary energy dependence on the crystallite lattice orientations on either side of the boundary, g and g', is shown along with the dependence on the boundary plane normal orientation, $\mathbf{n}$. The areal dependence on $\mathbf{n}$ is also indicated in the equation as the boundary area of a bamboo structure line decreases as $\mathbf{n}$ aligns with the direction of the interconnect line. Minimization of the total grain-boundary energy requires minimization of γ_{gb} as well as minimization of boundary area. These equations suggest that structure evolution may be partially controlled by grain-boundary energy considerations. Similar arguments can be made for surface energy and metal/oxide interface energy minimization. The optimal structure will achieve a total minimum energy based on each of these considerations.

Although γ_{gb} has been studied extensively, it is not well defined. Symmetric tilt boundaries about a low index plane are generally considered to be low-energy boundary types.[34–37] In addition, coincident site lattice (CSL) theory is often used as a criterion for identifying low-energy boundary types (cf. Refs. 20, 24 and 38). Data from the present investigation suggest that for (111)-oriented grains, the (110) planes tend to align with the grain-boundary plane, and the (211) plane forms the free-surface edges of the lines. This tends to support a third theory suggested by Wolf, where he concludes that asymmetrical grain boundaries, with a low-index plane on one side of the boundary, have lower energies than symmetrical boundaries on related high-index planes.[39] This means that for a (111)-oriented grain, the grain boundary may be in a low-energy configuration with a (110) plane aligned with the boundary, regardless of the lattice orientation of the adjoining crystallite. Simulations of grain growth with variable boundary energies indicate that preferred boundary structures may develop in interconnect lines.[40] One investigation suggests the existence of a preferred in-plane orientation in very narrow Au lines.[41] In this case, the sidewall orientations were preferentially (110) instead of (112), as suggested by the data presented in this report. Considering that the surface energies of these two planes is quite similar in fcc materials and they are at 90° from each other in the (111) plane, it is reasonable to conclude that either position

will provide a local minima in both boundary and surface energy, assuming a perfect bamboo structure.

The result for the damascene process fabricated specimens was inverse to that observed for the conventionally processed lines. The strength of the (111) fiber texture weakened as the linewidths decreased. This is likely due to the increasing effect of nucleation and growth on the sidewalls of the trenches with decreasing width. The trenches were 1 μm in depth and the growth of grains from these sidewalls during the deposition process was significant for lines of 2 μm width and less. The geometric constraint of linewidth was not a significant effect for the damascene processed specimens, as all lines were constrained by the trenches themselves.

Similar to the conventionally processed material, the damascene processed lines also contain an inordinate fraction of low angle grain boundaries as determined from the comparison of directly measured and uncorrelated misorientation distributions. These results undoubtedly stem from the competing mechanisms of surface energy, metal/oxide interface energy, and grain-boundary energy considerations. No trends were observed that indicate a preferred boundary structure in this material. The weaker texture and additional constraint of the sidewalls of the trenches likely constrains the narrow lines and may not allow for a preferred boundary structure dependence to develop. Analysis of the misorientation distribution functions in Rodrigues space indicates a linewidth dependence for the boundary structure, but this can be explained entirely using arguments based upon the observed texture differences. The narrow lines possess a weaker microtexture than the wider lines in that the distribution contains elements of (111)/(100)-type grain boundaries in addition to (111)-misoriented grains. This result is expected from analysis of the texture as both (111) and (100) components are observed in the distribution.

The distribution of rotation axes observed from the MDF calculations along with the observation of a propensity for (110) planes to be aligned with the grain-boundary plane in many specimens hints at some further analysis of these data and a more complete investigation of the processes involved for the conventionally processed specimens. The large majority of minimum angle rotation axes is concentrated near the $\langle 111 \rangle$ position. Those distributions, which are not completely of the $\langle 111 \rangle$ type, however, contain a secondary peak about the $\langle 110 \rangle$ axis. In addition, the distribution of crystallite lattice planes aligned with the grain boundary is generally weighted heaviest near the (110) position. (110) planes are relatively high-density planes in the fcc structure, though not in a close-packed arrangement like the (111) planes. These (110) positions provide for the highest density of lattice sites available in an orientation normal to the (111) pole aligned with the specimen normal direction. These (110) planes are those that possess the lowest surface energy, although the (211) poles are not far behind. The low-energy configuration is to have the (110) pole aligned with the interconnect line and the (211) being mutually orthogonal to the (111) and (110). Switching the positions of the (211) and (110) will have only a minimal effect on the energy of the system. It should again be stressed that all metal lines examined were bare, without passivation or encapsulation. Passivation will certainly provide additional constraints on structure evolution and different stress states on the lines, which could result in different preferred orientations.

No failure tests were performed on any of the specimens discussed in the present work, therefore, the data cannot be correlated to integrated circuit interconnect line reliability. However, from current knowledge of failure processes, a few hypotheses can be formulated. The weaker textures in the narrow damascene process fabricated lines suggest that these lines may be less reliable under electromigration conditions than the wider lines even though the structure of the narrow lines is near bamboo in character. The mixed texture components offer regions of fast diffusion intermixed with slow diffusion regions, which will result in more rapid electromigration failures.[1,4] The conventionally processed lines exhibit an inverse dependence of texture strength with linewidth, so the narrow lines will likely be more reliable under conditions where electromigration is likely to occur. The boundary-structure observations indicate that the preferred structure is for a (110) plane to be aligned with the grain boundary. This structure will likely result in a more reliable interconnect in two ways. First, the boundary is assumed to be in the preferred, low-energy position, making the boundary and surrounding structure more stable. Second, the [110] direction will be aligned with the interconnect line. As the system undergoes thermal fluctuations, the largest resolved shear stress of the thermal strains in the interconnect lines will be along the direction of the line and, therefore, along the [110] direction. This is the direction of easy glide on the (111) plane and may offer sufficient stress relaxation through anelastic or plastic deformation to improve reliability of the interconnect.

V. CONCLUSIONS

The investigation described above facilitates a number of conclusions about the texture and grain-boundary structure of conventionally processed and damascene processed interconnect lines. (111) fiber texture strength is inversely proportional to linewidth in conventionally processed structures subsequent to a postpatterning anneal, while it is proportional to linewidth for damascene processed fabricated lines. The distribution of low angle boundaries is highest for the stronger textured, narrow lines as compared with the wider lines. There exists a large fraction of low angle boundaries in all damascene processed and conventionally fabricated lines as compared with that which would occur for a random spatial distribution of texture components. Finally, for very narrow lines from conventional processing, a weak in-plane orientation preference suggests that the (110) lattice plane aligns preferentially with the grain boundary for the (111) fiber textured lines investigated.

ACKNOWLEDGMENTS

The authors acknowledge assistance from M. M. Nowell of TexSEM Laboratories in data collection and analysis. Helpful discussions with C. V. Thompson of MIT and P. S. Ho of UT Austin are also gratefully acknowledged.

[1] S. Vaidya and A. K. Sinha, Thin Solid Films **75**, 253 (1981).
[2] A. N. Campbell, R. E. Mikawa, and D. B. Knorr, J. Electron. Mater. **22**, 589 (1993).
[3] D. B. Knorr, Mater. Res. Soc. Symp. Proc. **309**, 75 (1993).
[4] D. B. Knorr and K. P. Rodbell, J. Appl. Phys. **79**, 2409 (1996).
[5] K. T. Lee, J. A. Szpunar, and A. Morawiec, Can. Metall. Q. **34**, 225 (1995).
[6] O. V. Kononenko, E. D. Ivanov, V. N. Matveev, and I. I. Khodos, Scr. Metall. Mater. **33**, 1981 (1995).
[7] B. L. Adams, S. I. Wright, and K. Kunze, Metall. Trans. **24**, 819 (1993).
[8] N. C. Krieger-Lassen, K. Conradsen, and D. Juul-Jensen, Scanning Microsc. **6**, 115 (1992).
[9] S. I. Wright, J. Comput.-Assisted Microsc. **5**, 207 (1993).
[10] S. Kordic, R. A. M. Wolters, and K. Z. Troost, J. Appl. Phys. **74**, 5391 (1993).
[11] D. P. Field, D. J. Dingley, M. M. Nowell, and B. L. Adams, Proc. ISTFA **21**, ASM International, p. 49 (1995).
[12] J. L. Hurd, K. P. Rodbell, D. B. Knorr, and N. L. Koligman, Mater. Res. Soc. Symp. Proc. **343**, 653 (1994).
[13] D. L. Barr, W. L. Brown, M. A. Marcus, and M. Ohring, Mater. Res. Soc. Symp. Proc. **391**, 347 (1995).
[14] S. Matthies and G. W. Vinel, Mater. Sci. Forum **157-162**, 1641 (1994).
[15] J. Pospiech, K. Sztwiertnia, and F. Haessner, Textures Microstruct. **6**, 201 (1986).
[16] J-W. Zhao, B. L. Adams, and P. R. Morris, Textures Microstruct. **8&9**, 493 (1988).
[17] D. P. Field and D. J. Dingley, J. Electron. Mater. **25**, 1767 (1996).
[18] J. K. Mackenzie, Biometrika **45**, 229 (1958).
[19] C. Turnbull and R. E. Hoffman, Acta Metall. **2**, 419 (1954).
[20] A. P. Sutton and R. W. Balluffi, Acta Metall. **35**, 2177 (1987).
[21] T. Watanabe, Mater. Sci. Forum **11**, 284 (1988).
[22] H. J. Frost, Y. Hayashi, C. V. Thompson, and D. T. Walton, Mater. Res. Soc. Symp. Proc. **338**, 295 (1994).
[23] D. Gupta, in *Diffusion Phenomena in Thin Films and Microelectronic Materials*, edited by D. Gupta and P. S. Ho (Noyes, Park Ridge, NJ, 1988), pp. 1–72.
[24] H. Grimmer, H. Bollmann, and D. D. Warrington, Acta Crystallogr. Sect. A **30A**, 197 (1974).
[25] D. G. Brandon, Acta Metall. **14**, 1479 (1966).
[26] W. Liu, M. Bayerlein, H. Mughrabi, A. Day, and P. N. Quested, Acta Metall. Mater. **40**, 1763 (1992).
[27] P. R. Besser, J. E. Sanchez, Jr., and D. P. Field, Mater. Res. Soc. Symp. Proc. (to be published).
[28] P. R. Besser, J. E. Sanchez, Jr., and D. P. Field, Proc. Advanced Metallization for ULSI, 1996. To be published.
[29] F. C. Frank, Metall. Trans. A **19**, 403 (1988).
[30] A. Morawiec and D. P. Field, Philos. Mag. A **73**, 1113 (1996).
[31] M. McLean and B. Gale, Philos. Mag. **20**, 1033 (1969).
[32] J. C. M. Li, J. Appl. Phys. **33**, 2958 (1962).
[33] W. T. Read and W. Shockley, Phys. Rev. **78**, 275 (1950).
[34] A. H. King and K. E. Harris, Mater. Sci. Forum **204-206**, 355 (1996).
[35] V. Randle, Acta Crystallogr. Sect. A **50**, 588 (1994).
[36] V. Singh and A. H. King, Scr. Metall. Mater. **34**, 1723 (1996).
[37] D. Wolf, Acta Metall. Mater. **38**, 781 (1990).
[38] H. Mykura, in *Grain Boundary Structure and Kinetics* (American Society for Metals, Metals Park, OH, 1979), p. 445.
[39] D. Wolf, Acta Metall. Mater. **38**, 791 (1990).
[40] H. J. Frost, Y. Hayashi, C. V. Thompson, and D. T. Walton, Mater. Res. Soc. Symp. Proc. **338**, 295 (1994).
[41] C. C. Wong, H. I. Smith, and C. V. Thompson, Mater. Res. Soc. Symp. Proc. **47**, 35 (1985).